Biogeosciences Discuss., 12, 16755–16801, 2015
www.biogeosciences-discuss.net/12/16755/2015/
doi:10.5194/bgd-12-16755-2015

Biogeosciences Discussions
Open Access

Benthic phosphorus cycling in the Peruvian oxygen minimum zone

U. Lomnitz[1], S. Sommer[1], A. W. Dale[1], C. R. Löscher[2], A. Noffke[3], K. Wallmann[1], and C. Hensen[1]

[1]GEOMAR Helmholtz Centre for Ocean Research Kiel, Wischhofstr. 1–3, 24148 Kiel, Germany
[2]Institute of General Microbiology, Christian Albrechts University Kiel, Kiel, Germany
[3]Institut für Seenforschung (ISF) der LUBW, Argenweg 50/1, 88085 Langenargen, Germany

Received: 15 September 2015 – Accepted: 17 September 2015 – Published: 19 October 2015

Correspondence to: U. Lomnitz (ulomnitz@geomar.de)

Published by Copernicus Publications on behalf of the European Geosciences Union.

Abstract

Oxygen minimum zones (OMZs) that impinge on continental margins favor the release of phosphorus (P) from the sediments to the water column, enhancing primary productivity and the maintenance or expansion of low-oxygen waters. A comprehensive field program in the Peruvian OMZ was undertaken to identify the sources of benthic P, including the analysis of particles from the water column, surface sediments and pore fluids as well as in situ benthic flux measurements. A major fraction of solid phase P was bound as particulate inorganic P (PIP) both in the water column and in sediments. Sedimentary PIP increased with depth in the sediment at the expense of particulate organic P (POP). The ratio of particulate organic carbon (POC) to POP exceeded the Redfield Ratio both in the water column (202 ± 29) and in surface sediments (303 ± 77). However, the POC to total particulate P (TPP = POP + PIP) ratio was close to Redfield in the water column (103 ± 9) and in sediment samples (102 ± 15) taken from the core of the OMZ. This observation suggests that the burial efficiencies of POC and TPP are similar under the low oxygen conditions prevailing in the Peruvian OMZ. Benthic fluxes of dissolved P were extremely high (up to $1.04 \pm 0.31\,\mathrm{mmol\,m^{-2}\,d^{-1}}$) and exceeded the fluxes resulting from the degradation of particulate organic matter raining to the seabed. Most of the excess P may have been released by bacterial mats that had stored P during previous periods when bottom waters were less reducing. At one station located at the lower rim of the OMZ, dissolved P was taken up by the sediments indicating recent phosphorite formation.

1 Introduction

Phosphorus is an essential nutrient; it serves as an energy carrier for all living species and is a limiting macronutrient for marine primary production on geological time scales (Filippelli, 2002; Föllmi, 1996; Ingall and Jahnke, 1994; McManus et al., 1997; Paytan and McLaughlin, 2007; Tsandev et al., 2012). Due to its impact on marine primary

BGD
12, 16755–16801, 2015

production, the oceanic phosphorus inventory modulates the atmospheric CO_2 level and earth's climate (Ganeshram et al., 2002; Ingall, 2010; Wallmann, 2003).

Particulate and dissolved phosphorus in the ocean originate from chemical weathering of the P containing mineral group of apatite on land (Filippelli, 2002). Only around 30 % of the P discharged to the oceans is potentially bioavailable (Compton et al., 2000) including dissolved P phases, inorganic P phases adsorbed to the surface of clay minerals or associated to Mn and Fe oxyhydroxides as well as P in particulate organic matter. However, the largest fraction of the delivered P is immediately trapped in estuaries or buried in continental margin sediments and thereby removed from the P cycle before it reaches the open ocean (Compton et al., 2000). P delivery to sediments in the open ocean is mainly composed of organic and inorganic P forms associated with the export of dead organic matter and other particles from the photic zone. Furthermore, P adsorbed to minerals as Mn and Fe oxyhydroxides or carbonate fluorapatites (CFA) is accumulated in the sediments (Delany, 1998; Faul et al., 2005; Föllmi, 1996). Additionally, P input to sediments by fish debris may be important in productive upwelling regions (Dìaz-Ochoa et al., 2009; Noffke, 2014; Schenau and DeLange, 2001; Suess, 1981).

P cycling is strongly affected by redox-dependent processes, due to the fact that P is typically scavenged by Fe oxyhydroxides. Reduction of Fe oxyhydroxides during anoxic diagenesis induces the release of phosphate across the sediment–water interface (Slomp et al., 1998; Sundby et al., 1986). Additionally, hypoxic or anoxic conditions favor the precipitation of P in the form of CFA (Froelich et al., 1988; Goldhammer et al., 2010; Ingall, 2010; Schenau and De Lange, 2000; Suess and von Huene, 1988). The resulting feedback on oceanic primary production triggered by changes in P release and P burial from anoxic sediments is still unclear. Presently, there are three opposing views in literature related to feedback mechanisms of the P cycling and its effect on the oceanic and atmospheric processes: (1) intensified phosphate release from the sediments to the water column caused by an expansion of low oxygen waters (Stramma et al., 2008) could stimulate the primary production in the surface waters (Wallmann,

BGD
12, 16755–16801, 2015

2003). This, in turn, may lead to a more intensified oxygen demand and a positive feedback with benthic P release (Moffit et al., 2015; Slomp and Van Cappellen, 2007; Wallmann, 2010). (2) A negative feedback scenario has been postulated based on the precipitation of CFA minerals found in the present-day oxygen depleted upwelling areas (Arning et al., 2009a, b; Cosmidis et al., 2013; Goldhammer et al., 2010; Schulz and Schulz, 2005). CFA mineral formation is a major sink for bioavailable P in marine environments (Delaney, 1998; Ingall, 2010). Hence, it is thought that the expansion of OMZs may increase the precipitation of CFA minerals in the sediments and outbalance the benthic phosphate release from anoxic sediments (Ganeshram et al., 2002; Goldhammer et al., 2010; Ingall, 2010). (3) A third scenario suggests that the formation of CFA is in balance with enhanced P release from anoxic sediments, implying that the dissolved oceanic P inventory is largely unaffected by oxygen concentrations (Anderson et al., 2001; Delaney, 1988; Roth et al., 2014). These conflicting scenarios show that there is further need to explore the benthic-pelagic P cycling in oxygen deficient environments in order to enable improved predictions.

We address this topic using a comprehensive data set from the Peruvian OMZ to identify P sources to the sediment. Our data set comprises samples of particulate matter from the water column as well as pore water and sediment samples. We present in situ benthic phosphate fluxes, particulate matter C/P ratios for water column particles and surface sediments and P burial fluxes for 6 stations along the depth transect across the Peruvian shelf at 12° S. From the data, we derive a mass balance for P cycling, resolving the input of P, P burial and benthic P release.

2 Study area

The study area is located in the center of the Peruvian OMZ at 12° S covering the shallow shelf from ~ 70 m water depth to mid-slope depths of about at ~ 400 m (Fig. 1). During our sampling campaign in January 2013 neutral or slightly negative El Niño–Southern Oscillation (ENSO) conditions dominated (http://www.cpc.ncep.noaa.gov)

BGD
12, 16755–16801, 2015

and the bottom water oxygen concentrations were below detection limit down to ~ 450 m water depth (Fig. 1, Table 1). Below the OMZ, oxygen concentrations rise to 19 and 53 µM at 770 and 1025 m water depth, respectively. Nitrate concentrations were below 12 µM from 128 to 407 m water depth (Table 1). During the measuring period, the bottom water at station I (74 m) was sulfidic and depleted in nitrate (Table 1; Sommer et al., 2015).

The oxygen deficient waters off Peru belong to one of the world's most prominent OMZs. Southeasterly trade winds that are driven by the Pacific Subtropical Anticyclone engender offshore transport of surface waters and upwelling of subsurface waters from the poleward propagating Peru undercurrent (PUC) (Strub et al., 1998). These water masses are oxygen depleted and rich in nutrients, favoring primary production of up to 3.6 g C m^{-2} d^{-1} in surface waters (Pennington et al., 2006). As a consequence, the intense oxygen consumption induced by the degradation of sinking particulate organic matter and a sluggish ventilation induce the development of a strong OMZ. Based on the definition that the oxycline of an OMZ is at ~ 22 µM (Fuenzalida et al., 2009), the Peruvian OMZ extends from approximately 50–700 m water depth. The greatest upwelling strength is reached during austral winter and spring between 5 and 15° S (Strub et al., 1998). The phases of strong upwelling are followed by high primary productivity rates in austral summer. The coastal area off Peru is a highly variable regime underlying the ENSO. Especially during positive ENSO periods coastal trapped waves emerging from equatorial Kelvin waves in the equatorial East Pacific occur frequently (Gutiérrez et al., 2009 and references therein). Consequently, the thermocline and the oxycline shift for 100 m and more downwards and oxygen concentration variations from 0 to 100 µM can occur in the timespan of days to weeks (Guitérrez et al., 2008; Schunck et al., 2013). The shelf area above 200 m water depth is therefore characterized by non-steady state conditions, whereas the oxygen concentrations in the core OMZ (~ 200–400 m water depth) are predominantly below the detection limit of 5 µM throughout the year.

The sediments of the Peruvian OMZ have POC contents ranging from 15–20 wt. % within the OMZ and > 5 wt. % on the shelf and below (Dale et al., 2015). The fine-

BGD
12, 16755–16801, 2015

grained, diatomaceous mud lens between 11 and 15° S accumulate under low PUC bottom water velocities in 50 to 500 m water depth (Krissek et al., 1980) This favors high sedimentation rates, carbon preservation and burial (Suess et al., 1987; Dale et al., 2015). Further down, at mid-slope depth, a high energy regime favoring erosive settings leads to the formation of phosphorites (Glenn and Arthur, 1988; Arning et al., 2009b; Reimers and Suess, 1983).

3 Methods

Sampling of water column particulate matter and sediment cores as well as the deployment of the benthic landers BIGO I and II (Biogeochemical Observatories) was conducted along the 12° S depth transect during the RV *Meteor* cruise M92 in January 2013. The geographical position and water column properties for the main stations are reported in Table 1. The dataset on in situ phosphate fluxes comprised 10 stations from 74 to 989 m water depth. The water column particle sampling was performed at 6 stations from 74 to 407 m water depth. These stations are considered as main stations and for consistency the stations are numbered according to the data set published in Dale et al. (2015). Hydrographic parameters and oxygen concentrations were obtained by deploying a CTD/rosette equipped with a Seabird oxygen sensor (detection limit is 5 µM) calibrated by Winkler titration.

3.1 Water column particles

Particulate matter was filtered using water from Niskin bottles from the CTD/rosette and analyzed for total particulate phosphorus (TPP), particulate inorganic phosphorus (PIP) and particulate organic carbon (POC) concentrations. Between three and six water depths were sampled per station. The water was filled into 10 L cans rinsed with ultrapure water (MilliQ) before. The cans were shaken before filtration which was performed within 24 h after sample retrieval. Approximately 2 to 4 L of sea water were

BGD
12, 16755–16801, 2015

filtered through pre-weighed and combusted (450 °C, 5 h) 0.7 µM Whatman GF/F filter using a sea water vacuum pump and Duran bottle top filters. After filtration, all filters were immediately frozen at −20 °C. At the shore-based laboratory the GF/F filters were dried over night at 45 °C, and divided into 3 equal sized pieces using a scalpel. The total filtered water volume was divided by three to calculate elemental concentrations on each filter section assuming homogenous coverage of particles on the filters.

3.1.1 Total particulate phosphorus (TPP), particulate inorganic phosphorus (PIP) and particulate organic phosphorus (POP)

The determination of TPP and PIP concentrations by combustion and colorimetric methods was described by Asahi et al. (2014), Aspila et al. (1976), Loh and Bauer (2000) and others. Filter segments for TPP concentration were combusted at 550 °C for 90 min and afterwards soaked with 20 mL 1 N hydrochloric acid (HCl) and shaken for 24 h at room temperature. Then, the solution was filtered and 0.35 mL triple reagent (40 mL 9.8 N sulfuric acid, 12 mL ammonium molybdate and 4 mL potassium antimonyl tartrate solution) and 0.175 mL ascorbic acid and 3 mL 1 N HCl were added to 0.75 mL of the standard. Before colorimetric measurement of phosphate at 880 nm using a Hitachi U-2001 photospectrometer the standard solution was neutralized for the HCl by 0.3 mL 12.5 N sodium hydroxide (NaOH) in order to adjust the pH. Measurements were conducted using a standard series ranging from 5 to 100 µM. The samples were measured undiluted due to low concentrations and the technical detection limit of a 1 cm cuvette. Hence, we used 3.75 mL of the filtered sample solution, added the reagents mentioned above and divided the concentrations by a factor of 5 to adjust the measurements to the ones of the standard series:

TPP/PIP [µmol L^{-1}] = (measured concentration/5 · 0.02)/(1/3 of the amount of filtered water)

The same procedure was performed for PIP without the combustion step. The POP concentration was calculated by the difference of the measured (as phosphate) TPP and PIP concentrations.

BGD
12, 16755–16801, 2015

3.1.2 Organic carbon concentration

The filter sections for the analysis of POC concentration were fumed with 37 % HCl overnight to remove inorganic carbon, dried and wrapped into tin caps. Samples were measured by flash combustion with a Carlo Erba elemental analyzer (NA1500). The analytical precision and detection limit amounted to 0.04 dry weight percent (%).

3.2 Pore water and solid phase analysis

Sediment cores were recovered using video-guided multiple corers (MUC) equipped with PVC liners with an inner diameter of 10 cm. The pore water and solid phase subsampling was performed immediately after recovery in an argon-filled glove bag at in situ sea floor temperature. The bottom water was siphoned with a plastic tube and filtered through cellulose acetate filters. Afterwards, the cores were sectioned into 0.5 cm intervals from 0–5 cm sediment depth and 1 cm intervals afterwards. The sediment samples were filled into centrifuge tubes and the pore water was separated from the sediments by centrifuging for 20 min at 4500 rpm. The supernatant pore water was filtered through cellulose acetate filters inside the glove bag. Samples were immediately analyzed for total dissolved phosphate (TPO_4) and dissolved ferrous iron (Fe^{2+}) after pore water extraction using a Hitachi U-2001 spectrophotometer. The analyses were performed according to the standard techniques described in Grasshoff et al. (1999). A sediment subsample was taken from each sediment depth and stored refrigerated in pre-weighed air-tight plastic cups to determine the water content, porosity and total organic carbon (TOC) content. The residual sediments were stored frozen or refrigerated for land-based analytics.

TOC content of freeze-dried and ground sediment samples was determined by flash combustion in a Carlo Erba Elemental Analyzer (NA 1500). Solid phase TPP and PIP concentrations were measured according to the method of Aspila et al. (1976) in a similar manner as described before for the water column particles. 50 mg of freeze-dried and ground sediment were digested in 1N HCl for a minimum of 24 h to dissolve

BGD
12, 16755–16801, 2015

the sedimentary PIP phase. Sediment portions analyzed for TPP were combusted at 550 °C for 90 min before adding 1 N HCl. The solutions were filtered and the reagents mentioned before were added before measurement. We used the sedimentary reference standards SDO-1 (Devonian Ohio Shale, USGS; Govindaraju, 1994) and MESS-3 (Marine Sediment Reference Material, Canadian Research Council) and replicate measurements of samples to ensure measurement accuracy. The standard series applied to the measurements covered a concentration range from 5 to 100 µM.

To determine terrigenous P input flux to the sediments, and to calculate the TPP burial flux, sediments were analyzed using total digestion. About 100 mg of freeze dried and ground sediment was digested in hydrofluoric acid (40 %, supra pure), nitric acid (65 %, supra pure) and perchloric acid (60 %, supra pure). For measurement accuracy the reference standards SDO-1 and MESS-3 as well as method blanks were included in the analysis. The aluminum concentration in the digestion solutions were measured using an inductively coupled plasma optical emission spectrometer (ICP-OES, Varian 720 ES). The relative standard deviation (RSD) for [Al] was found to be < 1 %.

The XRD data of core 107MUC23 from 407 m water depth were obtained from approximately 1 g of freeze dried and ground sediment in the lab of the University of Bremen.

3.3 POC in relation to various fractions of P (POC/*x*P ratios)

The molar POC/*x*P ratios (where *x*P = TPP, PIP and POP) of the water column particles at stations I, IV and V were calculated from two independent sample measurements per water depth. For these samples a minimum and maximum value was calculated. For the other stations III, VI and VIII, it was only one sample per water depth available. Here, we assumed an average error calculated from the duplicate measurements of stations I, IV and V for each P species (Supplement). For sediment samples we calculated a standard deviation for each station (Supplement).

BGD
12, 16755–16801, 2015

3.4 Benthic lander fluxes

Benthic lander deployments were performed at 10 stations along the 12° S transect (I to X according to Dale et al., 2015). In situ benthic fluxes were obtained using the two BIGOs I and II (BIGO). They were equipped with two circular flux chambers (internal diameter 28.8 cm, area 651.4 cm^2) (Sommer et al., 2009). An online video-controlled launch system allowed precise placement of the chambers at the seafloor directly located beneath the particle sampling stations in the water column and in proximity to the multi-corer stations. After a 2 h rest at the seafloor during which surrounding bottom water was periodically flushed into the chamber, the chambers were slowly driven into the sediment. The BIGOs stayed for 28 h at the seafloor, while 8 water samples per chamber were taken via glass syringes. In order to obtain bottom water background information, additional samples were taken every 8 h from the ambient bottom water. Phosphate concentrations in the syringe samples were measured on board using an auto analyzer. The standard series covered a concentration range from 0.05 to 3.5 µM. The fluxes were calculated from the slope of linear regression of all 8 data points vs. the sampling time (Supplement) and corrected for the water volume in the chamber and the dead volume of the 1 m long Vygon tubes connecting the syringes with the flux chambers. The error caused by the dilution from the dead volume of these tubes was calculated from the chloride concentration measured in the syringe samples. Benthic lander TPO_4 fluxes for most sites are based on two replicate chamber measurements. The uncertainty given for the TPO_4 fluxes is the difference between the minimum and maximum fluxes from the average of the two benthic chambers. At two stations (IV and V), it was only possible to calculate the flux from one chamber. For further details on the benthic flux measurements during the M92 cruise see Dale et al. (2015).

BGD
12, 16755–16801, 2015

3.5 Diffusive flux calculations

The diffusive fluxes of TPO_4 and Fe^{2+} from the sediment to the bottom water were calculated by applying Fick's First Law of diffusion:

$$F_{TPO4/Fe2+} = -\phi D_{SED}(d[C]/dx) \quad (1)$$

where the term $d[C]/dx$ describes the concentration gradient between the bottom water and the first pore water sample of the surface sediment divided by the sediment depth (0.25 or 0.5 cm) and ϕ is the porosity of the surface sediment. The diffusion coefficient, D_{SED}, for sediments was calculated according:

$$D_{SED} = D_{SW}/\theta^2 \quad (2)$$

The diffusion coefficients for TPO_4 and Fe^{2+} under standard conditions (D_{SW}) was taken from Li and Gregory (1974) and corrected for the in situ temperature and pressure using the Stokes–Einstein equation. The tortuosity (θ^2) was derived from the sediments porosity according to Boudreau (1996):

$$\theta^2 = 1 - \ln(\phi^2) \quad (3)$$

3.6 Mass balance of benthic phosphorus cycling

To investigate benthic P cycling quantitatively, a mass balance was developed considering P input, P burial, and P release. The equations for the P mass balance calculations are shown in Table 2. Under steady state conditions, the total P rain rate should balance the P buried in the sediments and the benthic TPO_4 flux (Table 2, Eq. 4). The rain rates of particulate P delivered to the sediments are differentiated in inorganic P (RR_{PIP}) (Table 2, Eq. 5) and organic P (RR_{POP}) (Table 2, Eq. 6). The rates were calculated using the POC/xP ratio of the water column particles that were taken as close as possible to the sea floor at each station (2–5 m above) and the POC rain rate (RR_{POC})

BGD
12, 16755–16801, 2015

(Table 4 and Supplement). RR_{POC} for the same stations along the 12° S transect were previously calculated by Dale et al. (2015) as the sum of the measured benthic DIC flux and the POC accumulation rate at 10 cm sediment depth. The terrigenous P input (RR_{Pterr}) (Table 2, Eq. 7) can be estimated by multiplying the solid phase aluminum concentration of the first sediment centimeter with the mass accumulation rate (Dale et al., 2015) and a P/Al ratio of 0.02 that characterizes the P/Al ratio of riverine transported particles originating from the continents (Viers et al., 2009).

The P burial flux (F_{Pbur}) (Table 2, Eq. 8) was calculated by multiplying the mass accumulation rate and the average solid phase P concentration of the first 10 sediment centimeter. The sediment mass accumulation rate (MAR) (Table 2, Eq. 9) was calculated from the sedimentation rate (SR in cm yr^{-1}), dry bulk density (ρ_{dry} in g cm^{-3}) and the average porosity of the sediments at the lower core end (ϕ_{∞}). Sedimentation rates were determined from particle-bound $^{210}Pb_{xs}$ measurements using a modeling approach. A detailed method description and the values used for this work are published in Dale et al. (2015). The error derived from modeling the sedimentation rate was given as 20 % and propagates to all subsequent calculations where it was used.

3.7 Freeze/thaw experiments

In order to determine the amount of polyphosphate stored in sulfide-oxidizing bacteria, foraminifera and other bacteria we conducted additional sediment experiments at all transect stations, except station IV. Sediments from MUC corers were sliced into 1 cm thick slices from the surface sediment to 10 cm sediment depth. Before phosphate analysis, sediments slices were repeatedly frozen at −80 °C and defrosted in order to burst microbial cells and release the internally stored P to the pore water.

3.8 Molecular quantification of filamentous bacteria

In order to quantify the abundance of filamentous microbes at the benthic boundary layer, we used a molecular approach. Nucleic acid purification was performed on

BGD
12, 16755–16801, 2015

0.5 g sediment following established protocols (Bertics et al., 2013). DNA was quality checked on an agarose gel and quantified using a Nanodrop spectrophotometer (Peqlab, Erlangen, Germany). A 16S rDNA PCR was performed with universal primers 27F and 1492R and obtained fragments were Topo TA cloned using the Topo TA cloning Kit (Invitrogen, Carlsbad, USA) and Sanger sequenced as previously described (e.g. Löscher et al., 2012). Sequencing was carried out in the Institute of clinical molecular biology at Kiel University. Sequences were analyzed using a Clustal W alignment tool on Mega 6 (Tamura et al., 2013) and deposited on GenBank (2015). A qPCR primer and probe set was established using the Primer Express software (Life Technologies, Carlsbad, USA) with the forward primer 5′ AGAAGCACCGGCTAACTCTG-3′, the reverse primer, 5′-TCGAATTAAACCACA-3′ and the probe 829-Thioploca 5′-GGATTAATTTCCCCCAACAT-3′ (Teske et al., 1995). Primers and probes were tested in silico on the Silva database and cross amplification was excluded on a variety of 16S rDNA clones. The qPCRs were performed in technical duplicates on a ViiA7 system (Life Technologies, Carlsbad, USA) as previously described (Löscher et al., 2014) using 1 × TaqMan PCR buffer (Life Technologies, Carlsbad, USA), 100 nM TaqMan probe, 5 pmol μL^{-1} of each primer, 400 ng μL^{-1} bovine serum albumin (to avoid PCR inhibition without affecting standard curves or detection limits), 3 µL PCR water, and 5 µL of either standard or environmental sample. A plasmid containing the target sequence was used to generate a standard dilution series for absolute quantification. The melting temperature was set to 50 °C. A theoretical detection limit of 4 copies per PCR reaction has been calculated. The results of the analysis are given in copies g^{-1} whereas a copy of the target 16S gene is equal to a single organism of *Thioploca spp*.

BGD
12, 16755–16801, 2015

4 Results

4.1 P composition of water column particulate matter

POC/POP ratios

The molar POC/POP ratios of the water column particles and of the surface sediments were consistently higher than the Redfield ratio at all stations (Fig. 2). The average POC/POP ratio of the water column particles was 202 ± 29. There was no clear trend through the water column, except slightly increasing ratios close to the seafloor. In the surface sediments, the ratios increased with the analyzed 0 to 6 cm of sediment depth, except at station VIII, with an average POC/POP ratio of 303 ± 77.

POC/PIP ratios

The average POC/PIP ratio of the water column particles was 248 ± 34. Similar to the POC/POP ratios, there was no significant trend through the water column. At the majority of the stations, the ratios decreased close to the seabed. The average POC/PIP ratio of the surface sediments was 184 ± 34 and almost constant over depth. In the sediments the ratios showed no significant down-core trend. At station VIII the ratio drastically decreased to an average of 7, similar to the POC/TPP ratios (below).

POC/TPP

The POC/TPP ratios of the water column particles and surface sediments consistently ranged around the Redfield ratio, with the exception of the sedimentary ratios at the shallowest (Sta. I, 74 m) and the deepest stations (Sta. VIII, 407 m). At station I the sediment measurements indicated significantly lower ratios than Redfield with an average of 69 in the surface sediments. The average POC/TPP ratio of the surface sediments at station VIII was 7. Close to the seabed, the POC/TPP ratios were stable or slightly increasing, with exception of station VIII where the ratios decreased sharply.

BGD
12, 16755–16801, 2015

4.1.1 PIP and POP fractions of TPP

The PIP fraction made up a large portion (21 to 74 %) of TPP in the water column particles (Fig. 3), as observed in previous studies (Benitez-Nelson et al., 2007; Faul et al., 2005; Lyons et al., 2011; Paytan et al., 2003; Sekula-Wood et al., 2012). The PIP fraction in the sediments reached 48 to 98 %. In comparison to the water column particles, the average sedimentary PIP fraction of TPP increased at each station, except at station VI. However, the strongest effect occurred at station VIII where the sedimentary PIP fraction comprised 98 % of TPP. XRD data from that station revealed that 7–16 wt. % of the sediments consisted of apatite and other phosphates (data not shown).

4.2 In situ benthic chamber fluxes

The benthic lander TPO_4 fluxes (F_{TPO_4}) are presented in Table 3 and Fig. 4a. Positive fluxes are defined as directed from the sediments into the water column. The highest TPO_4 flux along the depth transect of about $1.04 \pm 0.31\,mmol\,m^{-2}\,d^{-1}$ occurred at station I at 74 m water depth. Below 74 m water depth, fluxes decreased at least by a factor of 3 from 100 to 144 m water to 0.2–0.3 $mmol\,m^{-2}\,d^{-1}$. Measurements at 198 m water depth show a slightly increased TPO_4 flux of $0.44 \pm 0.07\,mmol\,m^{-2}\,d^{-1}$, while the fluxes measured at 244 and 306 m water depth decrease to the before mentioned levels. At 407 m water depth fluxes became negative, indicating a phosphate uptake by the sediment. At the stations below the OMZ (Sta. IX, 756 m and Sta. X, 989 m water depth), the fluxes increased to slightly positive values, but remain low at 0.06 and $0.02 \pm 0.02\,mmol\,m^{-2}\,d^{-1}$.

4.2.1 Comparison of benthic chamber TPO_4 fluxes and diffusive TPO_4 fluxes

The measured benthic chamber TPO_4 fluxes and the calculated diffusive TPO_4 fluxes show large discrepancies. The diffusive fluxes are consistently higher than the benthic

BGD
12, 16755–16801, 2015

fluxes (Fig. 4b). In contrast to the in situ measured benthic chamber TPO_4 release rates, the calculation of diffusive TPO_4 fluxes relies on bottom water and pore water PO_4^{3-} concentrations. A subsurface PO_4^{3-} peak occurs at all stations in the uppermost depth interval at 0–0.25 cm causing a large concentration gradient between the bottom water and the pore water PO_4^{3-} concentrations. The measured benthic TPO_4 fluxes exceed the fluxes that could be triggered by the TPP by a factor of approximately 6, but the potential TPO_4 fluxes are still higher (Table 4). Hence, the diffusive TPO_4 flux will be referred to as potential TPO_4 flux in the following.

4.3 TPP burial fluxes and TPP burial efficiency

The P burial fluxes reported in Table 4 decrease with increasing water depth. Station I has by far the highest P burial flux at 10 cm sediment depth with 0.23 mmol m^{-2} d^{-1}. In contrast the P burial efficiency at this station (Eq. 10) was comparatively low reaching only approximately 26 %. At Station VIII, the P burial flux is 0.03 mmol m^{-2} d^{-1} and the P burial efficiency exceeds 100 % due to the uptake of dissolved P from ambient bottom waters.

4.4 Molecular methods

Gene sequencing revealed that the filamentous sulfur bacteria in the surface sediments (0–5 cm) were *Thioploca ingrica*. By now, Thioploca was described to have one single 16S rDNA gene. Hence, the number of copies of this gene per g sediment can be directly translated into the abundance.

Their abundance decreased with increasing water depth (Table 4). Its highest abundance with more than 4000 copies g^{-1} sediment was found at station I, decreasing by more than a factor of 20 to 190 copies g^{-1} sediment at station VIII.

BGD
12, 16755–16801, 2015

5 Discussion

5.1 POC/*x*P ratios in water column particles and sediments

In order to characterize the fate of P in oxygen deficient waters and anoxic sediments we determined POC/*x*P ratios from both environments. Previous studies were focused either on the water column or on the sediments (Anderson et al., 2001 and references therein; Benitez-Nelson et al., 2004; Faul et al., 2005; Jilbert et al., 2011; Lyons et al., 2011; Sekula-Wood et al., 2012). The present data set provides a more complete insight of P compositional changes between the water column and surface sediment. Furthermore, it allows us to more rigorously constrain the sedimentary P mass balance compared to earlier studies (Ingall and Jahnke, 1994; Kraal et al., 2012; Mort et al., 2010; Noffke, 2014).

Both water column particles and the surface sediments from the Peruvian OMZ have POC/POP ratios above the Redfield ratio, indicating depletion in organic P relative to organic C. Such deviations have been previously reported (Benitez-Nelson et al., 2004; Faul et al., 2005; Franz et al., 2012; Loh and Bauer, 2000 and others) with different theories postulated to interpret these findings. In agreement, studies over large oxic water columns have demonstrated preferential depletion of organic P, both in the particulate and dissolved phases. These studies showed that phosphate diesters are preferentially solubilized, leading to POC/POP ratios ranging from 276 to 1138, with a mean value of 318 in diverse settings (Faul et al., 2005; Paytan et al., 2003). This was also reported for anoxic sediments (Anderson et al., 2001 and references therein), but there are no indications for such an effect on particulate matter in an anoxic water column (Bentiez-Nelson et al., 2004). Our results support this idea. We found constant POC/POP ratios that where above Redfield from 10 m water depth to the seabed which indicates similar degradation rates of POC and POP in the OMZ water column.

The high POC/POP ratios exceeding the Redfield value throughout the water column may reflect the composition of the Peruvian phytoplankton communities and their specific nutrient requirements as previously proposed by Franz et al. (2012) or may

BGD
12, 16755–16801, 2015

be induced by the microbial loop overprinting the primary phytoplankton stoichiometry already at shallow water depths. However, it could not be excluded yet that preferential POP over POC remineralization occurs in water depth < 10 m.

In contrast to the POC/POP ratio, water column POC/TPP ratios were close to the Redfield ratio. This could be an effect of surface adsorbed P that was previously described by Sanudo-Wilhelmy et al. (2004). Those authors investigated different species of *Trichodesmium* from the Atlantic Ocean. They found that the intracellular pool is strongly depleted in P, while the intracellular and the surface adsorbed P together are close to the Redfield ratio. Measurements of the internal P pool itself revealed strongly elevated C/P ratios compared to Redfield ratio. Our measurements are probably pointing in the same direction, but we did not differentiate between internal and external P pools. The existence of two distinct cellular P pools could have significant implications for studies using the Redfield model to define phytoplankton nutrient limitations. For example, the POC/TPP ratio implies an overestimation of the fraction of biologically available P, because TPP includes non-bioavailable phases such as detrital P (Anderson et al., 2001; Faul et al., 2005). Detrital P content can comprise 15 to 40 % of TPP in coastal areas (Filippelli, 1997). Due to the absence of measurements of the different PIP species it is not presently possible to quantify the detrital P in our samples.

Interestingly, increasing POC/POP ratios occur close to the seabed at all stations of the transect, with a further increase in the first sediment sample in 0–0.5 cm sediment depth indicating preferential POP remineralization relative to POC (Table 4, Fig. 2). Coincident with this, there is a decrease in POC/PIP ratios between the lowest water column sample and the surface sediments at all stations along the depth transect indicating an enrichment of PIP relative to POC (Fig. 2). This observation supports the hypothesis that organic P phases are converted into inorganic P phases which was previously described as sink switch effect (Faul et al., 2005; Ruttenberg and Berner, 1993). However, it remains unknown whether this process is limited to the uppermost sediment surface or takes also place in the bottom water. Since, the particle residence time in the bottom waters is comparable short, this effect is probably more apparent

BGD
12, 16755–16801, 2015

in the sediments. The analysis of the surface sediments along the depth transect also suggests preferential POP over POC remineralization within the investigated upper 5 cm of the surface sediments at 5 of 6 stations as the sedimentary POC/POP ratios increase with sediment depth at stations I, III, IV, V and VI (Fig. 2). This finding is consistent with previous studies reporting preferential POP over POC remineralization in anoxic sediments (Ingall et al., 1993; Ingall and Jahnke, 1994; Ingall, 2010; McManus et al., 1997; Van Cappellen and Ingall, 1996).

Sedimentary POC/TPP ratios were close to Redfield, except at the shallowest and deepest station. Thus, the sink switching mechanism where POP is converted into PIP while the TPP content of the sediment is conserved operates efficiently under low oxygen conditions. At first sight this observation seems to be inconsistent with the hypothesis that low oxygen conditions promote the release of dissolved P from sediments (Van Cappellen and Ingall, 1996). However, it should be noted that marine sediments covered by oxygen-bearing bottom waters feature molar POC/TPP ratios ranging from about 10 to 50 (Baturin, 2007). These ratios are much lower than Redfield because P is retained in sediments via adsorption and authigenic mineral precipitation while POC is efficiently degraded under aerobic conditions (Wallmann, 2010). Hence, our data set implies that a lack of oxygen eliminates the difference between POC and TPP burial efficiency. Hence, the close to Redfield POC/TPP ratio is likely due to both the enhanced preservation of POC in the Peruvian OMZ (Dale et al., 2015) and the release of dissolved P under low oxygen conditions.

5.2 P mass balance

P release rates from sediments underlying oxygen deficient waters are strongly enhanced compared to oxygenated marine settings, especially in the Peruvian OMZ (Noffke et al., 2012). Nonetheless, the sources for the enhanced P release are still not completely identified. The widely held view is that POP raining from the water column to the sediments represents the main source for sedimentary P in high productive areas like the Peru upwelling system (Delaney, 1998; Filippelli, 2008). Mass balance

BGD
12, 16755–16801, 2015

approaches that resolve the P regeneration vs. burial in oxygen deficient environments by combining sedimentary data and benthic P fluxes are rare (Ingall and Jahnke, 1994; Kraal et al., 2012; Mort et al., 2010; Noffke, 2014). These studies are all based on sediment data only, that is, the external P input to the sediments is estimated or ignored. Furthermore, the study areas were often not covered by fully anoxic bottom waters. Noffke (2014) presented an approach that combines measurements of solid phase P speciation, sediment burial fluxes and benthic chamber flux measurements for a mass balance on benthic P cycling in the Peruvian OMZ. Interestingly, the measurements on the solid phase P speciation revealed that organic P accounted for only 18–37 % of the total sedimentary P on the shelf and upper slope (Noffke, 2014). Furthermore, it was found that P bound to Fe oxyhydroxides and detrital P was of minor importance for the total sedimentary P inventory. However, authigenic Ca-P with a high amount of fish-P accounted for up to 47 % of the total P in sediments down to 300 m water depth and for up to 70 % in sediments below 300 m water depth. Consequently, Noffke (2014) suggested that authigenic Ca-P phases are an additional major P source besides organic P for benthic P release in the Peruvian OMZ.

Their mass balance approach was solely based on benthic work and has large uncertainties regarding the particulate P input from the water column. Our approach includes the particulate organic and inorganic P input from the water column, benthic P flux measurements and the P burial fluxes and is based on the steady state assumption that the P input has to be sufficient to maintain the benthic P flux and P burial flux. The P mass balance calculations (Table 4) illustrate the variability in TPO_4 release and burial as well as in the magnitude of particulate organic (Fig. 5a) and particulate inorganic P input (Fig. 5b) across the transect. Following the general assumption that POP is the major P phase delivered to the sediments (Delaney, 1998; Filippelli, 2008), we first calculated whether the rain rate of POP (RR_{POP}) to the seafloor can account for the measured benthic P fluxes (F_{TPO_4}) and P burial fluxes (F_{Pbur}) (Fig. 5a, Table 4). However, as already suggested in the first-order estimate of Noffke et al. (2012) and in Noffke (2014), the POP fraction is by far too small to balance the measured ben-

BGD
12, 16755–16801, 2015

thic fluxes in the Peruvian OMZ. The POP rain rates calculated along the transect can account for only 24 to 48 % of the measured TPO_4 fluxes (Fig. 5a), suggesting the likely presence of a source of inorganic P (Noffke, 2014). Similar to previous studies (Benitez-Nelson et al., 2007; Faul et al., 2005; Lyons et al., 2011; Paytan et al., 2003; Sekula-Wood et al., 2012), we found that the PIP fraction in water column particles ranging from 75 to 407 m water depth comprises between 21–74 % of TPP (Fig. 3). In the sediments, the average PIP fraction rises to 48–98 % of TPP (Fig. 3). Furthermore, POC and PIP were correlated (r^2 = 0.74) in the water column particles indicating highly reactive material. The mass balance approach including the particulate inorganic phosphorus rain rate to the seafloor (Fig. 5b) allows the depth transect to be divided into two sections. The first (station I, 74 m and III, 128 m) is characterized by high P input and release rates. The calculations on the P budget show a balance between the particulate P input, the benthic P fluxes and the P burial fluxes within the error margin (±20 %). In transect section two (stations IV, 141 m; V, 195 m and VI, 244 m), the P input decreases drastically (Fig. 5b, Table 4) whereas the benthic P fluxes are still comparatively high. The distinct mismatch in P input and P output prevails as the particulate P rain rates only support 37 to 61 % of the measured TPO_4 fluxes and calculated burial fluxes. This leads to the question: what drives the excess TPO_4 release in the core of the Peruvian OMZ?

5.2.1 Additional P input

Besides the P containing particulate matter raining from the water column to the sediments, there are other P sources that have to be considered. First, riverine transported material from the continent is a source of P to the sediments. The terrigenous P input was calculated using the mass accumulation rate of Al within the first centimeter of sediment and an average molar P/Al ratio of 0.02 ratio for riverine suspended particles (Viers et al., 2009). The resulting terrigenous P flux accounts for 5–19 % of the total P input which is insufficient to explain the observed discrepancies in the P budget of transect section II (Table 4, Figs. 4c and 5b).

BGD
12, 16755–16801, 2015

Laterally transported particles enriched in P from the very shallow shelf could be an additional P source (e.g. Jahnke, 1990). However, the particles would have to be strongly enriched in P, which is not the case. In addition, this would have to be reflected in the POC/TPP ratios of the surface sediments in transect section II (Fig. 2). The ratios are not or only slightly enriched in TPP compared to the water column particles leading to the conclusion that lateral transport of P-enriched particles to the sediments is an unlikely candidate for the missing P source.

Another alternative, is the existence of an additional PIP phase supplied by fast sinking material (e.g. P containing fish scales) that was not sampled during CTD casts, and hence is not present on our filter samples. Díaz-Ochoa et al. (2009) showed that fish P can make up to 20 % of the total sedimentary P inventory in the shelf sediments of the Peruvian OMZ. Hence, the fish P input should be depicted in strongly depleted sedimentary POC/TPP ratios compared to the water column particles which are not found, as described above. Theoretically sediments need to be composed of particles having POC/TPP ratios between 11 ± 1 and 25 ± 12 (Table 4) to maintain the measured P release rates in transect section II. It seems unlikely that the mismatch in the P mass balance is caused by additional particles deposited at the seabed since their POC/TPP ratio would need to be much lower than any value observed in our data set.

5.2.2 Non steady state scenarios – internal sedimentary P pools

Besides an additional P input to the sediments from the water column, regeneration of particulate P within the sediment could contribute to the excess P release (Noffke et al., 2012). This could include P released from the dissolution of Fe oxyhydroxides or the degradation of internally stored polyphosphates by sulfide-oxidizing bacteria. Such non-steady state scenarios can be induced by repeatedly occurring short term changes in the bottom water geochemistry. Annual changes like El Niño and La Niña events as well as internally occurring Kelvin waves cause oxygenation events and influence nutrient concentrations (Guitérrez et al., 2008).

BGD
12, 16755–16801, 2015

It is well known that the sedimentary cycles of Fe and P are strongly linked (Kraal et al., 2015) and the reductive dissolution of Fe oxyhydroxides leads to an enhanced PO_4^{3-} accumulation in the pore waters of anoxic sediments. A minimum estimate of TPO_4 released during the reduction of Fe oxyhydroxides can be calculated from the diffusive Fe^{2+} fluxes and the molar Fe/P ratio that is found in Fe oxyhydroxides. The diffusive Fe^{2+} fluxes were in the range of 0.03 to 0 mmol m^{-2} d^{-1} during the M92 cruise (Table 4). The molar Fe/P ratio of Fe oxyhydroxides is about 10 (Slomp et al., 1996). The calculation of the minimum TPO_4 release rates from Fe oxyhydroxides (Eq. 14) results in a maximum flux of 0.003 mmol PO_4^{3-} m^{-2} d^{-1} (Table 4, Figs. 4c and 5b), equivalent to less than 5 % of the benthic P flux and burial flux.

Another internally activated P pool is phosphate released from large sulfur-oxidizing bacteria, e.g. *Beggiatoa* (Brock and Schulz-Vogt, 2011; Sannigrahi and Ingall, 2005). These microorganisms store and release P (in the form of intracellular polyphosphate granules) under oscillating redox conditions and therefore it is generally assumed that they strongly affect benthic TPO_4 fluxes (Brock and Schulz-Vogt, 2011; Dale et al., 2013; Ingall and Jahnke, 1994; Sannigrahi and Ingall, 2005; Schulz and Jørgensen, 2005). Hence, polyphosphates are an important P pool in the sediments of highly productive upwelling areas (Kraal et al., 2015). Along the depth transect, dense mats of sulfur bacteria *Thioploca ingrica* were observed on the sediments during video-launched MUC and benthic lander deployments down to 300 m water depth (Dale et al., 2015). This was also previously described by Mosch et al. (2012) and references therein. Although, it is not confirmed that *Thioploca* spp. has a mechanism to store and degrade polyphosphates similar like its close relatives, the sulfur bacteria *Beggiatoa* spp. and *Thiomargarita* spp. (Holmkvist et al., 2010; Høgslund et al., 2009), our findings provide circumstantial indications that this is also applicable to *Thioploca* spp.

Firstly, we found that the abundance of copies of *Thioploca* per g^{-1} sediment and the measured benthic TPO_4 release rates have a linear relationship with a correlation factor of $r^2 = 0.92$ (Fig. 6). This finding may supports the suggestion that bacteria

BGD
12, 16755–16801, 2015

have a systematic control on benthic P fluxes. Secondly, a comparison of the in situ measured benthic P fluxes and the diffusive P fluxes calculated from the difference of the TPO_4 bottom water concentration and the TPO_4 pore water concentration of the surface sediments revealed great differences (Fig. 4b). Such a difference could be explained by the lysis of bacterial cells during sample retrieval followed by the release of the internally stored polyphosphate pool into the pore water. Following this argument, the diffusive P fluxes cannot be taken as real fluxes, but as a measure for potential maximum release rates of P by *Thioploca*. Moreover, the potential fluxes are by far sufficient to compensate for the missing P fraction in transect section II (ranging from 0.06 ± 0.02 to $0.3 \pm 0.04\,\mathrm{mmol\,m^{-2}\,d^{-1}}$; Table 4, Fig. 4c).

Additionally to the established pore water procedure, we carried out freeze/thaw experiments to quantify the amount of P stored in sulfide-oxidizing bacteria (see method Sect. 3.7). However using this method, it cannot be excluded that the P released during the procedure originates also from other bacteria and foraminifera in the sediments. The released polyphosphates from the microbial cells are rapidly hydrolyzed to orthophosphate under acidic conditions (Jager and Heyns, 1998). Hence, the standard method to determine phosphate in the pore waters using acidic reagents will likely support the hydrolysis of polyphosphates enabling us the measure its concentration in the pore waters after conducting the experiments. A comparison of the pore water phosphate concentrations and the experiment results show that the amount of the additionally released P is as twice as high as the pore water P concentration in transect section I and more than 10 times larger in section II (Fig. 7). Those results are coincident with the finding from the mass balance approach, where the largest discrepancies occur in transect section II and are another indication for the bacterial impact on the benthic P release.

It remains to be shown how these mechanisms play out in detail (e.g. nutrient concentration thresholds, time scales, P release from *Thioploca*) and the impact on benthic P release in oxygen and nitrate deficient environments on longer time scales. Summarizing the results of the mass balance it should be noted, that even with determining

BGD
12, 16755–16801, 2015

the particulate P rain rate from the water column to the sediments, the P mass balance for the core of the Peruvian OMZ is imbalanced and requires an additional P source to maintain the benthic TPO_4 fluxes and P burial fluxes.

5.2.3 Indications for active phosphorite formation

In contrast to the stations between 74 and 244 m water depth characterized by P release, data of station VIII at 407 m water depth indicate the uptake of phosphate from bottom water. To our best knowledge, this is the first time that a downward flux of dissolved phosphate from bottom waters into phosphorite-bearing surface sediments has been documented by in situ benthic flux measurements.

Arning et al. (2008) presented investigations on phosphorites that were recovered from the Peruvian OMZ including a station at 12° S from the same water depth (~ 400 m) and in close vicinity to sampling station VIII. The suboxic bottom waters and low sedimentation rates in that area seem to be favorable for phosphorite formation close to the sediment–water interface (Arning et al., 2009b). Cosmidis et al. (2013) suggested three mechanisms how high pore water phosphate concentrations that are essential for the phosphogenesis can be generated in the sediments: (1) remineralization of organic matter mainly through bacterial sulfate reduction releasing phosphate to the pore waters, (2) reductive dissolution of Fe oxyhydroxides and the release of adsorbed P and (3) use of internally stored polyphosphates by large sulfide-oxidizing bacteria. Using the same mass balance approach as presented before, we calculate a P accumulation rate of $33 \pm 4\,\mathrm{mmol\,m^{-2}\,yr^{-1}}$ at station VII where most of the P is derived from ambient bottom waters ($26\,\mathrm{mmol\,m^{-2}\,yr^{-1}}$). Hence, our data suggest that the phosphorite nodules at this station contain phosphate that originates predominantly from ambient bottom waters. Sediments at station VIII were covered by benthic foraminifera instead of mat-forming sulfur bacteria. The release of phosphate from frosted and defrosted samples from this site may indicate that these foraminifera are storing large quantities of polyphosphates in their cells (Fig. 7). Contrary to the findings of Goldhammer et al. (2010) and Schulz and Schulz (2005), our observations suggest

BGD
12, 16755–16801, 2015

that polyphosphate storing benthic foraminifera rather than bacterial mats might facilitate the uptake of bottom water phosphate and the formation of phosphorites at station VIII.

The P uptake rate derived from our lander measurements may be compared to previous estimates on phosphorite growth rates in the area. However, the latter approach is based on the dating of phosphoric laminites and yields a P uptake rate of only 3 mmol P m^{-2} yr^{-1} for a ca. 1 Ma old nodule (Arning et al., 2009a). This difference may be at least partly explained by the methodological difference (present flux measurement vs. long-term average), however, growth rates determined on modern nodules are broadly consistent with our flux measurements (Burnett et al., 1982).

6 Conclusions

This study aimed to identify the P sources of benthic P release in Peruvian OMZ. We determined the rain rates of organic particulate phosphorus and inorganic particulate phosphorus and determined benthic P release rates and P burial fluxes.

Our calculations revealed that in nearly all cases rain rates cannot compensate measured benthic fluxes and burial fluxes. Systematic analysis of potential P sources revealed that most likely P release form sulfide-oxidizing bacteria is (periodically) increasing benthic fluxes, and hence compensation for a missing P source. These bacteria store P when terminal electron acceptors for sulfide oxidation are available and release dissolved P during periods when these oxidants are scarce. We visited the area during austral summer when oxygen and nitrate levels were depleted by high export production and respiration. It is possible that the Peruvian OMZ was less reducing prior to our sampling period due to lower respiration rates and/or better ventilation. Thus, we propose that the bacterial mats act as a capacitor being unloaded during austral summer and recharged during other periods of the year when bottom waters are less reducing which was previously proposed in Dale et al. (2013). This hypothesis could be veri-

BGD
12, 16755–16801, 2015

fied/falsified by a systematic study of the seasonality of benthic fluxes in the Peruvian up-welling system.

In addition, measurements at the phosphorite station VIII showed clear indications for the uptake of dissolved phosphate by the sediments facilitating phosphorite formation. Our data imply that most of the P accumulating in these authigenic minerals originates from ambient bottom waters. Since this site was marked by a high abundance of P-bearing benthic foraminifera we speculate that phosphate uptake and phosphorite formation may be supported by these organisms.

POC/TPP ratios in both water column particles and sediments were close to Redfield at most sites in the Peruvian OMZ. This observation strongly suggests that the burial efficiencies of POC and TPP are similar under low oxygen conditions whereas TPP is better conserved than POC in the presence of oxygen (Wallmann, 2010). Thus, a lack of oxygen promotes the release of dissolved P from sediments and the preservation of POC (Dale et al., 2015) until both phases are buried at a ratio similar to Redfield.

Our data support the hypothesis that benthic P release triggers a positive feedback loop leading to intensified primary production in the surface water and enhanced oxygen demand specifically during periods where a lack of terminal electron acceptors in ambient bottom waters promotes the release of P from bacterial mats. However, this positive feedback is limited by the formation of authigenic inorganic P phases maintaining the long-term average POC/TPP burial ratio close to Redfield.

The Supplement related to this article is available online at doi:10.5194/bgd-12-16755-2015-supplement.

Author contributions. U. Lomnitz, A. W. Dale and S. Sommer supported the shipboard work, geochemical analysis and contributed to the manuscript preparations. C. Hensen, K. Wallmann and A. Noffke helped with fruitful discussions related to the manuscript and helped with the manuscript preparation. C Löscher carried out the molecular analysis and contributed to the manuscript.

BGD
12, 16755–16801, 2015

Acknowledgement. We are very grateful to the crew of RV *Meteor* during cruise M92 for the support of. Our thanks also go to A. Petersen, M. Türk and S. Cherednichenko for their assistance in deploying the landers. For their enthusiastic help and cooperation, we thank B. Domeyer, S. Kriwanek, A. Bleyer, R. Suhrberg, S. Trinkler and V. Thoenissen for biogeochemical analyses on board and in the home laboratory. Furthermore, we appreciate Christopher Voigt from the University of Bremen for carrying out XRD analysis. This work is a contribution of the Sonderforschungsbereich 754 "Climate – Biogeochemistry Interactions in the Tropical Ocean" (www.sfb754.de) which is supported by the Deutsche Forschungsgemeinschaft.

References

Anderson, L. D., Delaney, M. L., and Faul, K. L.: Carbon to phosphorus ratios in sediments: implications for nutrient cycling, Global Biogeochem. Cy., 15, 65–79, 2001.

Arning, E. T., Birgel, D., Schulz-Vogt, H. N., Holmkvist, L., Jørgensen, B. B., Larson, A., and Peckmann, J.: Lipid biomarker patterns of phosphogenic sediments from upwelling regions, Geomicrobiol. J., 25, 69–82, 2008.

Arning, E. T., Birgel, D., Brunner, B., and Peckmann, J.: Bacterial formation of phosphatic laminites off Peru, Geobiology, 7, 295–307, 2009a.

Arning, E. T., Lückge, A., Breuer, C., Gussone, N., Birgel, D., and Peckmann, J.: Genesis of phosphorite crusts off Peru, Mar. Geol., 262, 68–81, 2009b.

Asahi, T., Ichimi, K., Yamaguchi, H., and Tada, K.: Horizontal distribution of particulate matter and its characterization using phosphorus as an indicator in surface coastal water, Harima-Nada, the Seto Inland Sea, Japan, J. Oceanogr., 70, 277–287, 2014.

Aspila, K. I., Agemian, H., and Chau, A. S. Y.: A semi-automated method for the determination of inorganic, organic and total phosphate in sediments, Analyst, 101, 187–197, 1976.

Baturin, G. N. and Savenko, V. S.: Phosphorus in oceanic sedimentogenesis, Oceanology, 37, 107–113, 1997.

Benitez-Nelson, C. R.: The biogeochemical cycling of phosphorus in marine systems, Earth-Sci. Rev., 51, 109–135, 2000.

Benitez-Nelson, C. R., O'Neill, L., Kolowith, L. C., Pellechia, P., and Thunell, R.: Phosphonates and particulate organic phosphorus cycling in an anoxic marine basin, Limnol. Ocean., 49, 1593–1604, 2004.

BGD
12, 16755–16801, 2015

Benitez-Nelson, C. R., O'Neill Madden, L. P., Styles, R. M., Thunell, R. C., and Astor, Y.: Inorganic and organic sinking particulate phosphorus fluxes across the oxic/anoxic water column of Cariaco Basin, Venezuela, Mar. Chem., 105, 90–100, 2007.

Berelson, W. M., Hammond, D. E., and Johnson, K. S.: Benthic fluxes and the cycling of biogenic silica and carbon in two southern California borderland basins, Geochim. Cosmochim. Ac., 51, 1345–1363, 1987.

Berelson. W., McManus, J., Coale, K., Johnson, K., Burdige, D., Kilgore, T., Colodner, D., Chavez, F., Kudela, R., and Boucher, J.: A time series of benthic flux measurements from Monterey Bay, CA, Cont. Shelf Res., 23, 457–481, 2003.

Bertics, V. J., Löscher, C. R., Salonen, I., Dale, A. W., Gier, J., Schmitz, R. A., and Treude, T.: Occurrence of benthic microbial nitrogen fixation coupled to sulfate reduction in the seasonally hypoxic Eckernförde Bay. Baltic Sea. Biogeosciences. 10, 1243–1258, 2013.

Boudreau, B. P.: The diffusive tortuosity of fine-grained unlithified sediments., Geochim. Cosmochim. Ac., 60, 3139–3142, 1996.

Brock, J. and Schulz-Vogt, H. N.: Sulfide induces phosphate release from polyphosphate in cultures of a marine Beggiatoa strain, ISME J, 5, 497–506, 2011.

Burnett, W. C., Beers, M. J., and Roe, K. K.: Growth rates of phosphate nodules from the continental margin off Peru, Science, 215, 1616–1618, 1982.

Compton, J., Mallinson, D., Glenn, C., Filipelli, G., Föllmi, K., Shields, G., and Zanin, Y.: Variations in the global phosphorus cycle, in Marine authigenesis: from global to microbial, Sediment. Geol., 66, 21–33, 2000.

Cosmidis, J., Benzerara, K., Menguy, N., and Arning, E.: Microscopy evidence of bacterial microfossils in phosphorite crusts of the Peruvian shelf: implications for phosphogenesis mechanisms, Chem. Geol., 359, 10–22, 2013.

Dale, A., Bertics, W., V. J., Treude, T., Sommer, S., and Wallmann, K. Modeling benthic–pelagic nutrient exchange processes and porewater distributions in a seasonally hypoxic sediment: evidence for massive phosphate release by *Beggiatoa*?, Biogeosciences, 10, 629–651, 2003,
http://www.biogeosciences.net/10/629/2003/.

Dale, A. W., Sommer, S., Lomnitz, U., Montes, I., Treude, T., Liebetrau, V., Gier, J., Hensen, C., Dengler, M., Stolpovsky, K., Bryant, L. D., and Wallmann, K.: Organic carbon production, mineralisation and preservation on the Peruvian margin, Biogeosciences, 12, 1537–1559, doi:10.5194/bg-12-1537-2015, 2015.

BGD
12, 16755–16801, 2015

de Jager, H.-J., and Heyns, A. M.: Kinetics of acid-catalyzed hydrolysis of a polyphosphate in water, J. Phys. Chem.-US., 102, 2838–2841, 1998.
Delaney, M. L.: Phosphorus accumulation in marine sediments and the oceanic phosphorus cycle, Global Biogeochem. Cy., 12, 563–572, 1998.
Díaz-Ochoa, J. A., Lange, C. B., Pantoja, S., De Lange, G. J., Gutierrez, D., Munoz, P., and Salamanca, M.: Fish scales in sediments from off Callao, central Peru, Deep-Sea Res. Pt. II, 56, 1113–1124, 2009.
Faul, K. L., Paytan, A., and Delaney, M. L.: Phosphorus distribution in sinking oceanic particulate matter, Mar. Chem., 97, 307–333, 2005.
Filippelli, G. M.: Controls on phosphorus concentration and accumulation in oceanic sediments, Mar. Geol., 139, 231–240, 1997.
Filippelli, G. M.: The global phosphorus cycle, in phosphates: geochemical, geobiological, and materials importance, in: Reviews in Mineralogy & Geochemistry, edited by: Kohn, M., Rakovan, J. and Hughes, J., 391–425, 2002.
Filippelli, G. M.: The global phosphorus cycle: past, present, and future, Elements, 4, 89–95, 2008.
Föllmi, K. B.: The phosphorus cycle, phosphogenesis and marine phosphate-rich deposits, Earth-Sci. Rev., 40, 55–124, 1996.
Franz, J., Krahmann, G., Lavik, G., Grasse, P., Dittmar, T., and Riebesell, U.: Dynamics and stoichiometry of nutrients and phytoplankton in waters influenced by the oxygen minimum zone in the eastern tropical Pacific, Deep-Sea Res. Pt. I, 62, 20–31, 2012.
Froelich, P. N., Arthur, M. A., Burnett, W. C., Deakin, M., Hensley, V., Jahnke, R., Kaul, L., Kim, K. H., Roe, K., Soutar, A., Vathakanon, C.: Early diagenesis of organic matter in Peru continental margin sediments: phosphorite precipitation, Mar. Geol., 80, 309–343, 1988.
Fuenzalida, R., Schneider, W., Garcés-Vargas, J., Bravo, L., and Lange, C.: Vertical and horizontal extension of the oxygen minimum zone in the eastern South Pacific Ocean, Deep-Sea Res. Pt. II, 56, 992–1003, 2009.
Ganeshram, R. S., Pedersen, T. F., Calvert, S., and Francois, R.: Reduced nitrogen fixation in the glacial ocean inferred from changes in marine nitrogen and phosphorus inventories, Nature, 415, 156–159, 2002.
Glenn, C. R. and Arthur, M. A.: Petrology and major element geochemistry of Peru margin phosphorites and associated diagenetic minerals: authigenesis in modern organic-rich sediments, Mar. Geol., 80, 231–267, 1988.

BGD
12, 16755–16801, 2015

Goldhammer, T., Bruchert, V., Ferdelman, T. G., and Zabel, M.: Microbial sequestration of phosphorus in anoxic upwelling sediments, Nat. Geosci., 3, 557–561, 2010.
Govindaraju, K.: Compilation of working values and sample description for 383 geostandards, Geostandard Newslett., 18, 1–158, 1994.
Grasshoff, K., M. Erhardt, M., and Kremling, K.: Methods of Seawater Analysis, 3rd edn., Wiley-VCH, Weinheim, New York, Chiester, Brisbane, Singapore, Toronto, 1999.
Gutiérrez, D., Enríquez, E., Purca, S., Quipúzcoa, L., Marquina, R., Flores, G., and Graco, M.: Oxygenation episodes on the continental shelf of central Peru: remote forcing and benthic ecosystem response, Prog. Oceanogr., 79, 177–189, 2008.
Høgslund, S., Revsbech, N. P., Kuenen, J. G., Jorgensen, B. B., Gallardo, V. A., v. d. Vossenberg, J., Nielsen, J. L., Holmkvist, L., Arning, E. T., and Nielsen, L. P.: Physiology and behaviour of marine Thioploca, ISME J., 3, 647–657, 2009.
Holmkvist, L., Arning, E. T., Küster-Heins, K., Vandieken, V., Peckmann, J., Zabel, M., and Jørgensen, B. B.: Phosphate geochemistry, mineralization processes, and Thioploca distribution in shelf sediments off central Chile, Mar. Geol., 277, 61–72, 2010.
Ingall, E. D.: Biogeochemistry: phosphorus burial, Nat. Geosci., 3, 521–522, 2010.
Ingall, E. and Jahnke, R.: Evidence for enhanced phosphorus regeneration from marine sediments overlain by oxygen depleted waters, Geochim. Cosmochim. Ac., 58, 2571–2575, 1994.
Ingall, E. D., Bustin, R. M., and Van Cappellen, P.: Influence of water column anoxia on the burial and preservation of carbon and phosphorus in marine shales, Geochim. Cosmochim. Ac., 57, 303–316, 1993.
Ingall, E., Kolowith, L., Lyons, T., and Hurtgen, M.: Sediment carbon, nitrogen and phosphorus cycling in an anoxic fjord, Effingham Inlet, British Columbia, Am. J. Sci., 305, 240–258, 2005.
Jahnke, R. A.: Early diagenesis and recycling of biogenic debris at the seafloor, Santa Monica Basin, California, J. Mar. Res., 48, 413–436, 1990.
Jilbert, T., Slomp, C. P., Gustafsson, B. G., and Boer, W.: Beyond the Fe-P-redox connection: preferential regeneration of phosphorus from organic matter as a key control on Baltic Sea nutrient cycles, Biogeosciences, 8, 1699–1720, doi:10.5194/bg-8-1699-2011, 2011.
Kraal, P., Slomp, C. P., Reed, D. C., Reichart, G.-J., and Poulton, S. W.: Sedimentary phosphorus and iron cycling in and below the oxygen minimum zone of the northern Arabian Sea, Biogeosciences, 9, 2603–2624, doi:10.5194/bg-9-2603-2012, 2012.

BGD
12, 16755–16801, 2015

Kraal, P., Bostick, B. C., Behrends, T., Reichart, G.-J., and Slomp, C. P.: Characterization of phosphorus species in sediments from the Arabian Sea oxygen minimum zone: combining sequential extractions and X-ray spectroscopy, Mar. Chem., 168, 1–8, 2015.

Krissek, L. A., Scheidegger, K. F., and Kulm, L. D.: Surface sediments of the Peru-Chile continental margin and the Nazca plate, Geol. Soc. Am. Bull., 91, 321–331, 1980.

Li, Y.-H. and Gregory, S.: Diffusion of ions in sea water andin deep-sea sediments., Geochim. Cosmochim. Ac., 38, 703–714, 1974.

Loh, A. N. and Bauer, J. E.: Distribution, partitioning and fluxes of dissolved and particulate organic C, N and P in the eastern North Pacific and Southern Oceans, Deep-Sea Res. Pt. I, 47, 2287–2316, 2000.

Löscher, C. R., Kock, A., Könneke, M., LaRoche, J., Bange, H. W., and Schmitz, R. A.: Production of oceanic nitrous oxide by ammonia-oxidizing archaea, Biogeosciences, 9, 2419–2429, doi:10.5194/bg-9-2419-2012, 2012.

Lyons, G., Benitez-Nelson, C. R., and Thunell, R. C.: Phosphorus composition of sinking particles in the Guaymas Basin, Gulf of California, Limnol. Oceanogr., 56, 1093–1105, 2011.

McManus, J., Berelson, W. M., Coale, K. H., Johnson, K. S., and Kilgore, T. E.: Phosphorus regeneration in continental margin sediments, Geochim. Cosmochim. Ac., 61, 2891–2907, 1997.

Mort, H. P., Slomp, C. P., Gustafsson, B. G., and Andersen, T. J.: Phosphorus recycling and burial in Baltic Sea sediments with contrasting redox conditions, Geochim. Cosmochim. Ac., 74, 1350–1362, 2010.

Mosch, T., Sommer, S., Dengler, M., Noffke, A., Bohlen, L., Pfannkuche, O., Liebetrau, V., and Wallmann, K.: Factors influencing the distribution of epibenthic megafauna across the Peruvian oxygen minimum zone, Deep-Sea Res. Pt. I, 68, 123–135, 2012.

Noffke, A.: Phosphorus cycling in anoxic sediments, PhD dissertation, University of Kiel, Kiel, 2014.

Noffke, A., Hensen, C., Sommer, S., Scholz, F., Bohlen, L., Mosch, T., Graco, M., and Wallmann, K.: Benthic iron and phosphorus fluxes across the Peruvian oxygen minimum zone, Limnol. Oceanogr., 57, 851–867, 2012.

Paytan, A. and McLaughlin, K.: The oceanic phosphorus cycle, Chem. Rev., 107, 563–576, 2007.

Paytan, A., Cade-Menun, B. J., McLaughlin, K., and Faul, K. L.: Selective phosphorus regeneration of sinking marine particles: evidence from 31P-NMR, Mar. Chem., 82, 55–70, 2003.

BGD
12, 16755–16801, 2015

Pennington, J. T., Mahoney, K. L., Kuwahara, V. S., Kolber, D. D., Calienes, R., and Chavez, F. P.: Primary production in the eastern tropical Pacific: a review, Prog. Oceanogr., 69, 285–317, 2006.

Redfield, A. C., Ketchum, B. H., and Richards, F. A.: The influence of organisms on the composition of seawater, in: The Sea, Academic Press, London, 26–77, 1963.

Reimers, C. E. and Suess, E.: Spatial and temporal patterns of organic matter accumulation on the Peru continental margin, in: Coastal Upwelling: Part B. Sedimentary Record of Ancient Coastal Upwelling, edited by: Suess, E. and Thiede, J., Plenum Press, New York, 311–346, 1983.

Ruttenberg, K. C. and Berner, R. A.: Authigenic apatite formation and burial in sediments from non-upwelling, continental margin environments, Geochim. Cosmochim. Ac., 57, 991–1007, 1993.

Sannigrahi, P. and Ingall, E.: Polyphosphates as a source of enhanced P fluxes in marine sediments overlain by anoxic waters: evidence from 31P NMR, Geochem. T., 6, 52–59, 2005.

Sanudo-Wilhelmy, S. A., Tovar-Sanchez, A., Fu, F.-X., Capone, D. G., Carpenter, E. J., and Hutchins, D. A.: The impact of surface-adsorbed phosphorus on phytoplankton Redfield stoichiometry, Nature, 432, 897–901, 2004.

Schenau, S. J. and De Lange, G. J.: A novel chemical method to quantify fish debris in marine sediments, Limnol. Oceanogr., 45, 963–971, 2000.

Schenau, S. J. and De Lange, G. J.: Phosphorus regeneration vs. burial in sediments of the Arabian Sea, Mar. Chem., 75, 201–217, 2001.

Schulz, H. N. and Jørgensen, B. B.: Thiomargarita, in: Bergey's Manual of Determinative Bacteriology, edited by: Krieg, N. R., Staley, J. T., and Brenner, D. J., Vol. 2, part B, Springer-Verlag, Berlin, Heidelberg, New York, 169–171, 2005.

Schulz, H. N. and Schulz, H. D.: Large sulfur bacteria and the formation of phosphorite, Science, 307, 416–418, 2005.

Schunck, H., Lavik, G., Desai, D. K., Großkopf, T., Kalvelage, T., Löscher, C. R., Paulmier, A., Contreras, S., Siegel, H., Holtappels, M., Rosenstiel, P., Schilhabel, M. B., Graco, M., Schmitz, R. A., Kuypers, M. M. M., and LaRoche, J.: Giant hydrogen sulfide plume in the oxygen minimum zone off Peru supports chemolithoautotrophy, PLOS ONE, 8, 1–18, 2013.

Sekula-Wood, E., Benitez-Nelson, C. R., Bennett, M. A., and Thunell, R.: Magnitude and composition of sinking particulate phosphorus fluxes in Santa Barbara Basin, California, Global Biogeochem. Cy., 26, GB2023, doi:10.1029/2011GB004180, 2012.

BGD
12, 16755–16801, 2015

Slomp, C. P. and Van Cappellen, P.: The global marine phosphorus cycle: sensitivity to oceanic circulation, Biogeosciences, 4, 155–171, doi:10.5194/bg-4-155-2007, 2007.
Slomp, C. P., Van der Gaast, S. J., and Van Raaphorst, W.: Phosphorus binding by poorly crystalline iron oxides in North Sea sediments, Mar. Chem., 52, 55–73, 1996.
Slomp, C. P., Malschaert, J. F. P., and Van Raaphorst, W.: The role of adsorption in sediment-water exchange of phosphate in North Sea continental margin sediments, Limnol. Oceanogr., 43, 832–846, 1998.
Sommer, S., Linke, P., Pfannkuche, O., Schleicher, T., v. Deimling, S., Reitz, A., Haeckel, M., and Hensen, C.: Seabed methane emissions and the habitat of frenulate tubeworms on the Captain Arutyunov mud volcano (Gulf of Cadiz), Mar. Ecol.-Prog. Ser., 382, 69–86, 2009.
Sommer, S., Gier, J., Treude, T., Lomnitz, U., Dengler, M., Cardich, J. and Dale, A.: Depletion of oxygen, nitrate and nitrite in the Peruvian oxygen minimum zone cause an imbalance of benthic nitrogen fluxes, Deep-Sea Res. Pt. I, submitted, 2015.
Stramma, L., Johnson, G. C., Sprintall, J., and Mohrholz, V.: Expanding oxygen-minimum zones in the tropical oceans, Science, 320, 655–658, 2008.
Strub, P. T., Mesias, J. M., Montecino, V., Ontecino, R., and Salinas, S.: Coastal ocean circulation of western South America, in: The Sea, edited by: Robinson, A. R. and Brink, K. H., Wiley, 273–313, 1998.
Suess, E.: Phosphate regeneration from sediments of the Peru continental margin by dissolution of fish debris, Geochim. Cosmochim. Ac., 45, 577–588, 1981.
Suess, E. and von Huene, R.: Ocean Drilling Program Leg 112, Peru continental margin: part 2, sedimentary history and diagenesis in a coastal upwelling environment, Geology, 16, 939–943, 1988.
Suess, E., Kulm, L. D., and Killingley, J. S.: Coastal upwelling and a history of organic rich mudstone deposition off Peru, in: Marine Petroleum Source Rocks, edited by: Brooks, J. and Fleet, A. J., Geological Society Spec, London, 1129–1145, 1987.
Sundby, B., Anderson, L. G., Hall, P. O. J., Iverfeldt, Å., van der Loeff, M. M. R., and Westerlund, S. F. G.: The effect of oxygen on release and uptake of cobalt, manganese, iron and phosphate at the sediment–water interface, Geochim. Cosmochim. Ac., 50, 1281–1288, 1986.
Tamura, K., Stecher, G., Peterson, D., Filipski, A., and Kumar, S.: MEGA6, molecular evolutionary genetics analysis version 6.0., Mol. Biol. Evol., 30, 2725–2729, 2013.

BGD
12, 16755–16801, 2015

Teske, A., Ramsing, N. B., Küver, J., and Fossing, H.: Phylogeny of thioploca and related filamentous sulfide-oxidizing bacteria, Syst. Appl. Microbiol., 18, 517–526, 1995.

Tsandev, I., Reed, D. C., and Slomp, C. P.: Phosphorus diagenesis in deep-sea sediments: sensitivity to water column conditions and global scale implications, Chem. Geol., 330–331, 127–139, 2012.

Van Cappellen, P. and Ingall, E. D.: Redox stabilization of the atmosphere and oceans by phosphorus-limited marine productivity, Science, 271, 493–496, 1996.

Viers, J., Dupré, B., and Gaillardet, J.: Chemical composition of suspended sediments in world rivers: new insights from a new database, Sci. Total Environ., 407, 853–868, 2009.

Wallmann, K.: Feedbacks between oceanic redox states and marine productivity: a model perspective focused on benthic phosphorus cycling, Global Biogeochem. Cy., 17, 1084, doi:10.1029/2002GB001968, 2003.

Wallmann, K.: Phosphorus imbalance in the global ocean?, Global Biogeochem. Cy., 24, GB4030, doi:10.1029/2009GB003643, 2010.

BGD
12, 16755–16801, 2015

Table 1. Station list for the sites of the benthic lander (BIGO), multi-corer (MUC) and CTD deployments. Also shown are the bottom water concentrations of oxygen (O_2), nitrate (NO_3^-) and sulfide (H_2S). The station numbers were chosen for comparability according to Dale et al. (2015). bdl = below detection limit (5 µM).

Nr.	Station	Gear	Date (2013)	Longitude (° W)	Latitude (° S)	Water depth (m)	BW O_2 (µM)	BW NO_3^- (µM)	BW H_2S (µM)
	98	CTD26	14.01.	12°13.504′	77°10.799′	75			
I	220	MUC39	25.01.	12°13.531′	77°10.061′	72	bdl	–	33.22
	110	BIGO1-2	15.01.	12°13.506′	77°10.793′	74			
	269	CTD79	29.01.	12°16.690′	77°14.999′	128			
III	248	MUC46	27.01.	12°16.697′	77°15.001′	129	bld	0.02	–
	165	BIGO2-4	20.01.	12°16.690′	77°14.995′	128			
	111	CTD29	15.01.	12°18.729′	77°17.757′	145			
IV	36	MUC10	09.01.	12°18.708′	77°17.794	145	bdl	7.1	
	57	BIGO1-1	11.01.	12°18.711′	77°17.803′	141			
	279	CTD81	30.01.	12°21.490′	77°21.713′	195			
V	247	MUC45	27.01.	12°21.491′	77°21.702′	195	bdl	6.3	–
	201	BIGO1-4	23.01.	12°21.502′	77°21.712′	195			
	92	CTD24	13.01.	12°23.300′	77°24.200′	244			
VI	198	MUC34	23.01.	12°23.300′	77°24.228′	244	bdl	11.9	–
	74	BIGO2-2	12.01.	12°23.300′	77°24.186′	244			
	66	CTD16	12.01.	12°27.535′	77°29.593	414			
VIII	107	MUC23	15.01.	12°27.198′	77°29.497′	407	bdl	12.1	–
	207	BIGO2-5	24.01.	12°27.207′	77°29.517′	409			

BGD
12, 16755–16801, 2015

Table 2. Equations for the P mass balance calculations. Results are shown in Table 4.

Equations for P mass balance calculations		
P Input to the sediments (mmol m^{-2} d^{-1})		
(4)	Total particulate phosphorus rain rate	$RR_{TPP} = RR_{PIP} + RR_{POP} = F_{TPO_4} + F_{Pbur}$
(5)	Particulate inorganic phosphorus rain rate	$RR_{PIP} = RR_{POC} / (\frac{POC}{PIP})$
(6)	Particulate organic phosphorus rain rate	$RR_{POP} = RR_{POC} / (\frac{POC}{POP})$
(7)	Terrigenous P input	$RR_{Pterr} = Al_{0-1} \cdot MAR \cdot 0.02$
P Burial in the sediments (mmol m^{-2} d^{-1} and g m^{-2} d^{-1})		
(8)	Phosphorus burial flux	$F_{Pbur} = MAR \cdot P_{10}$
(9)	Mass accumulation rate	$MAR = \rho_{dry} \cdot (1 - \phi\infty) \cdot SR$
(10)	TPP burial efficiency	$PBE = MAR \cdot \frac{P_{10}}{RR_{TPP}} \cdot 100$
P release from the sediments (mmol m^{-2} d^{-1}) Benthic P fluxes (F_{TPO_4}) and the potential diffusive P fluxes were determined as descried above		
(11)	P release from POP degradation according to Redfield (C/P=106)	$F_{P(POP)} = F_{DIC}/106$
(12)	True P release from POP	$F_{P(POP)} = F_{DIC}/(\frac{POC}{POP})$
(13)	P release from total particulate phosphorus	$F_{P(TPP)} = F_{DIC}/(\frac{POC}{TPP})$
(14)	P release from the dissolution of Fe oxyhydroxides (Fe/P=10, Slomp et al., 1996)	$F_{P(FE)} = F_{Fe2+}/(\frac{Fe}{P})$ $F_{P(FE)} = F_{Fe2+}/(\frac{Fe}{P})$
(15)	P deficit to outbalance the P budget	$F_{P(deficit)} = (F_{TPO4} = F_{Pbur} - RR_{TPP} + RR_{terr} + F_{P(Fe)})$

BGD
12, 16755–16801, 2015

Table 3. In situ benthic chamber TPO_4 fluxes in mmol m^{-2} d^{-1} along the 12° S transect. The averages are given where both benthic chambers were completely recovered and the uncertainty corresponds to the mean difference between the minimum and maximum fluxes from the two benthic chambers.

Station		Water depth	F_{TPO_4}
		(m)	(mmol $m^{-2}d^{-1}$)
I	BIGO1_2	74	1.04 ± 0.31
II	BIGO1_5	101	0.35 ± 0.01
III	BIGO2_4	128	0.30 ± 0.05
IV	BIGO1_1	141	0.23[a]
V	BIGO1_4	195	0.12[a]
VI	BIGO2_2	243	0.44 ± 0.07
VII	BIGO2_1	306	0.26 ± 0.04
VIII	BIGO2_5	409	−0.07[a]
IX	BIGO2_3	756	0.06[a]
X	BIGO1_3	989	0.02 ± 0.02

[a] Only one benthic flux was measured.

BGD
12, 16755–16801, 2015

Table 4. Measured and calculated parameters for the P mass balance along the 12° S transect. The numbers in front of key parameters correspond to equations in Table 2.

	Transect section I				Transect section II						Phosphorite formation	
12° S	Station I 74 m		Station III 128 m		Station IV 141 m		Station V 195 m		Station VI 244 m		Station VIII 407 m	
Benthic chamber TPO_4 flux (F_{TPO_4})* mmol m^{-2} d^{-1}	1.04	±0.31	0.3	±0.05	0.23	–	0.12	–	0.44	±0.07	−0.07	–
Thioploca ingrica abundance[a] copies g^{-1} (0–5 cm sediment depth)	4159				1687		3072				190	
Benthic chamber DIC flux (F_{DIC})**W mmol m^{-2} d^{-1}	65.9	±21	20.4	±7	8	±0.4	3.2	±1	4.7	±1	2.2	±0.3
POC rain rate (RR_{POC})[b] mmol m^{-2} d^{-1}	79.5	±33	28.2	±12	10.5	±3	12.5	±6	10.6	±4	2.7	±1
Sediment accumulation rate (ω_{acc})[b] cm yr^{-1}	0.45	±0.09	0.2	±0.04	0.04	±0.008	0.1	±0.02	0.07	±0.014	0.01	±0.002
Mass accumulation rate (MAR)[b] g m^{-2} yr^{-1}	1800	±360	600	±120	128	±26	320	±64	182	±37	44	±9
ratios for particulate matter from the water column 2 to 5 m above the sea floor:												
POC:TPP	76	±4	68	±9	94	±10	132	±36	62	±9	96	±9
POC:PIP	197	±17	125	±34	291	±79	385	±7	217	±34	209	±34
POC:POP	126	±17	149	±29	142	±3	214	±87	87	±29	178	±29
(4) TPP rain rate (RR_{TPP}) mmol m^{-2} d^{-1}	1.00	±0.31	0.40	±0.09	0.11	±0.02	0.09	±0.02	0.17	±0.02	0.03	±0.01
(5) PIP rain rate (RR_{PIP}) mmol m^{-2} d^{-1}	0.39	±0.14	0.22	±0.04	0.04	±0	0.03	±0.02	0.05	±0.01	0.01	±0.01

BGD
12, 16755–16801, 2015

Table 4. Continued.

	Transect section I				Transect section II						Phosphorite formation	
12° S	Station I 74 m		Station III 128 m		Station IV 141 m		Station V 195 m		Station VI 244 m		Station VIII 407 m	
(6) POP rain rate (RR_{POP}) mmol m^{-2} d^{-1}	0.61	±0.18	0.18	±0.05	0.07	±0.02	0.06	±0.01	0.12	±0.01	0.01	±0.01
(7) Terrigenous P input (RR_{Pterr})	0.10	–	0.02	–	0.01	–	0.02	–	0.01	–	0.00	–
(8) Burial flux (F_{Pbur}) in 10 cm sediment depth mmol m^{-2} d^{-1}	0.23	–	0.08	–	0.05	–	0.05	–	0.04	–	0.03	–
Avg. Al conc. of 0–1 cm sediment depth (Al_{0-1})[a] mmol g^{-1}	0.99	–	0.70	–	1.10	–	0.97	–	0.72	–	0.66	–
Avg. P conc. of first 10 cm sediment depth (P_{10})[a] mmol g^{-1}	0.05	–	0.05	–	0.14	–	0.06	–	0.07	–	0.2	–
(10) P burial efficiency (PBE) at 10 cm sediment depth %	26	±8	20	±4	47	±8	61	±14	21	±3	106	±23
(11) P release from POP degradation according to Redfield ($F_{P(Red)}$) mmol m^{-2} d^{-1}	0.62	±0.2	0.19	±0.06	0.08	±0.01	0.03	±0.01	0.04	±0.02	0.02	±0
(12) P release from POP degradation ($F_{P(POP)}$) mmol m^{-2} d^{-1}	0.52	±0.16	0.14	±0.05	0.06	±0.01	0.02	±0.01	0.05	±0.02	0.01	±0
(13) P release from TPP degradation ($F_{P(TPP)}$) mmol m^{-2} d^{-1}	0.87	±0.17	0.3	±0.1	0.09	±0.01	0.02	±0.01	0.08	±0.02	0.02	±0.01
Benthic diffusive TPO_4 flux (potential P flux)[a]	1.08	±0.23	2.0	–	0.5	–	1.6	–	1.5	–	–	–
Diffusive Fe^{2+} flux (F_{Fe2+})[a]	0.04	±0.02	0.01		0.02		0.0		0.03		0.0	
(14) P released from Fe oxyhydroxides ($F_{P(Fe)}$)	0.004	±0.002	0.001		0.002		0.0		0.003		0.0	
(15) Potential bacterial P release ($F_{P(Bact)}$)	–		–		0.15	±0.02	0.06	±0.02	0.3	±0.04	–	

[a] Measured.
[b] published data from Dale et al. (2015).

BGD
12, 16755–16801, 2015

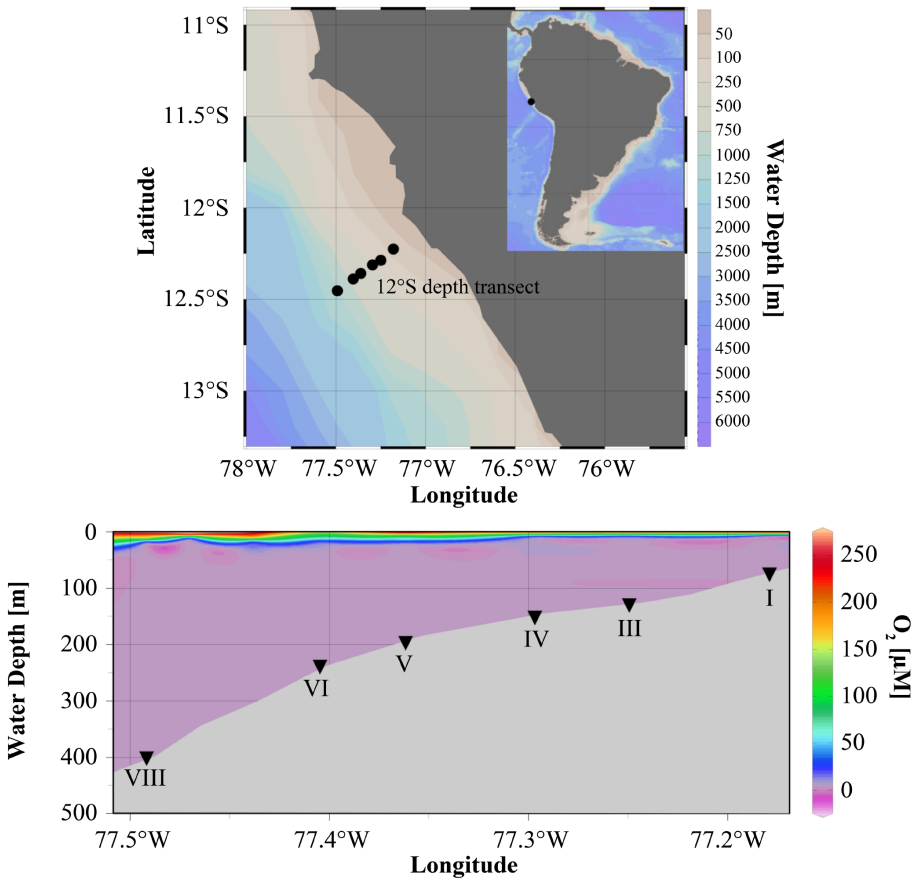

Figure 1. Study area, sampling stations and O_2 concentration along the 12° S transect.

BGD
12, 16755–16801, 2015

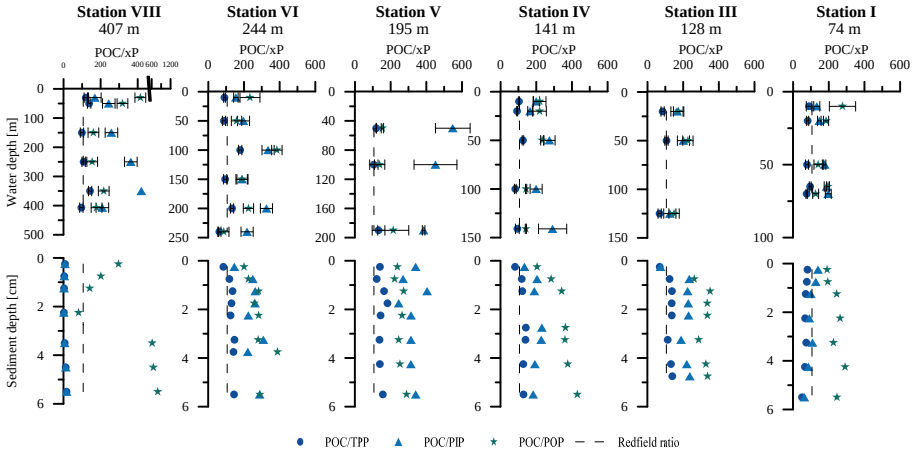

Figure 2. Ratios of POC to TPP, PIP and POP (POC/xP) along the 12° S depth transect from water column particles and sediments from 0–5.5 cm sediment depth of station I to VIII.

BGD
12, 16755–16801, 2015

Benthic phosphorus cycling in the Peruvian oxygen minimum zone

U. Lomnitz et al.

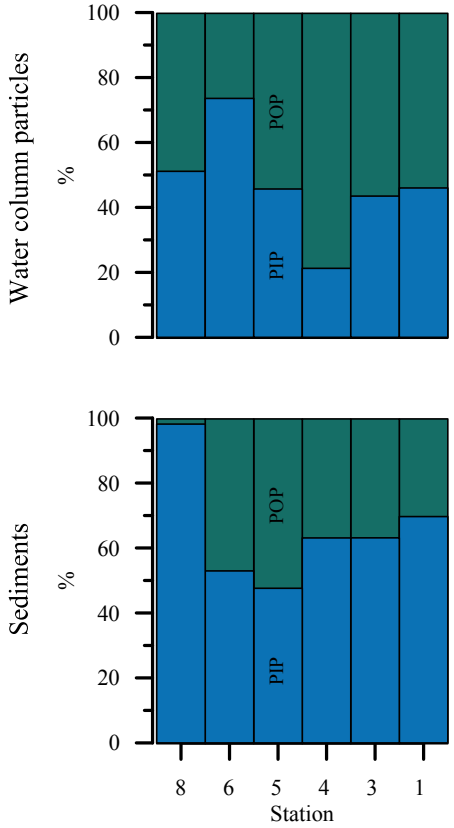

Figure 3. Average distribution of POP and PIP (%) per station in the water column particles and in the top 5 cm of the sediments.

BGD
12, 16755–16801, 2015

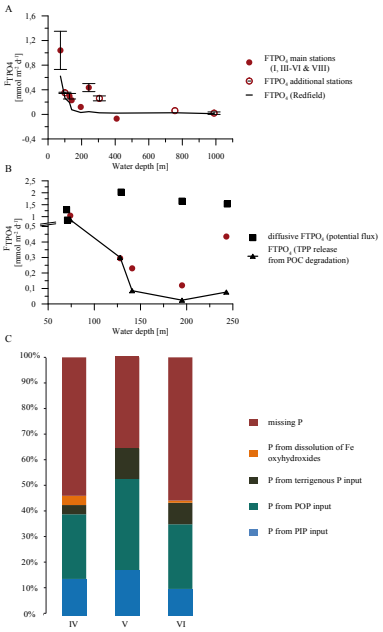

Figure 4. (a) Measured benthic TPO_4 fluxes at 12° S. The black line shows the theoretical TPO_4 flux generated from organic matter remineralization with a Redfield POC/POP ratio of 106, **(b)** potential TPO_4 fluxes from diffusive flux calculations compared to the measured benthic TPO_4 fluxes of the stations I to VIII. The black line with triangles depicts the TPO_4 flux that could be generated from the total particulate phosphorus by organic matter remineralization, **(c)** the bar chart illustrates the percentages of the different P input sources and the missing P that is needed to maintain the measured TPO_4 release rates and P burial fluxes for stations IV, V and VI of transect section II. The missing P is assumed to be supplied by sulfide-oxidizing bacteria *Thioploca ingrica*.

BGD
12, 16755–16801, 2015

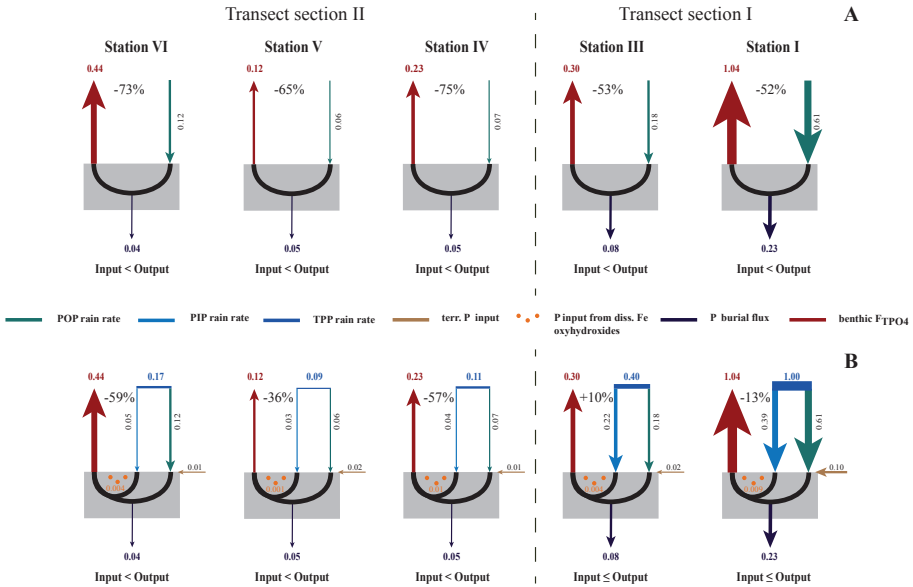

Figure 5. Mass balance calculations and measured benthic TPO_4 fluxes [mmol m^{-2} d^{-1}] for stations I to VIII, **(a)** POP rain rates, TPO_4 fluxes and P burial rates only. The number in percent depicts missing P needed to sustain the benthic TPO_4 fluxes, **(b)** mass balance calculations including the POP and PIP rain rates, the terrigenous P input, P release from the reductive dissolution of Fe oxyhydroxides and the benthic TPO_4 fluxes into the bottom waters as well as the P burial rates.

BGD
12, 16755–16801, 2015

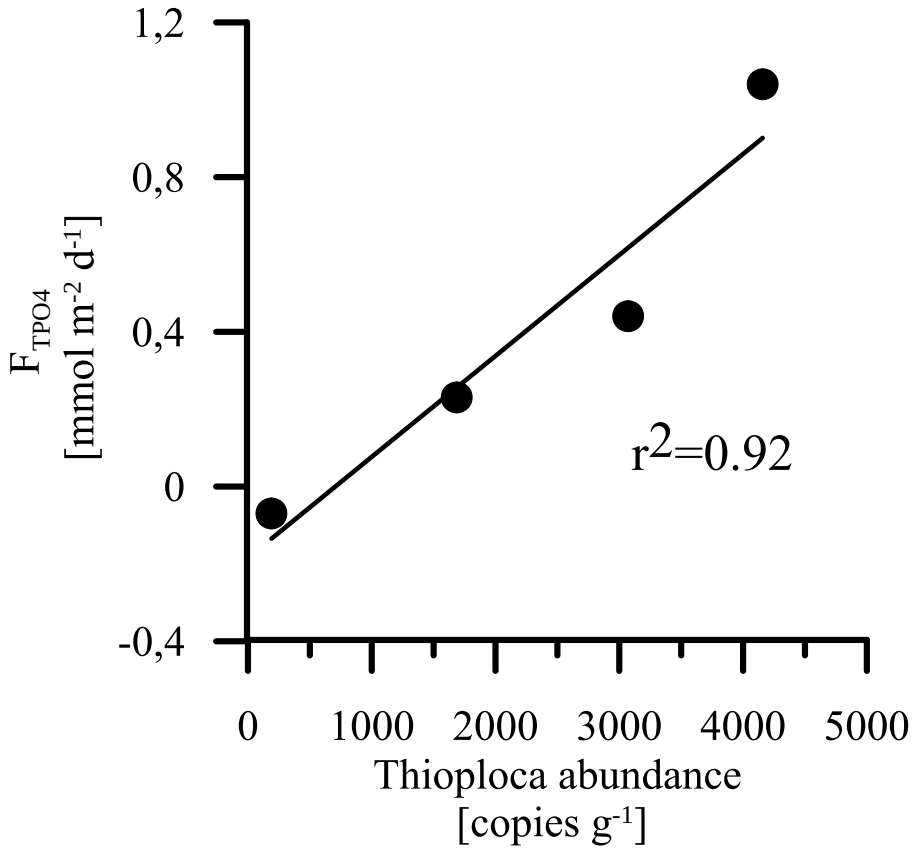

Figure 6. Abundance of *Thioploca* in cells g^{-1} in the first 5 cm of the sediment in correlation to the measured benthic TPO_4 fluxes. Highest abundance and TPO_4 flux was found at station I. The other data points are for the stations IV, VI and VIII (with decreasing abundance and TPO_4 flux).

BGD
12, 16755–16801, 2015

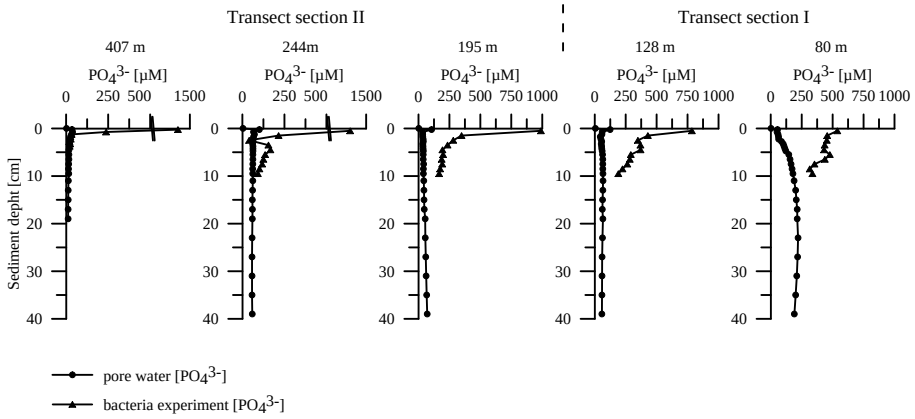

Figure 7. Comparison of pore water PO_4^{3-} concentrations before (circles) and after (triangles) the freeze/thawing experiments.

BGD
12, 16755–16801, 2015